2007 IEEE International Conference on
Robotics and Automation
Roma, Italy, 10-14 April 2007

A Humanoid Foot with Polypyrrole Conducting Polymer Artificial Muscles for Energy Dissipation and Storage

Thomas W. Secord, H. Harry Asada

Abstract— **This paper describes the design and analysis of a humanoid foot constructed using polypyrrole (PPy) conducting polymer (CP) actuators. The compliance and damping of natural muscles plays an important role in natural human gait. Conducting polymers actuators and other smart structure actuators can store energy by means of inherent mechanical compliance that traditional DC motor actuators do not possess. This paper presents a method for optimizing the inherent compliance and damping of the actuators in order to minimize the active control effort required to generate a natural human gait. A simplified kinematic model of the design is evaluated using biomechanical joint angle and ground reaction force (GRF) data to yield the desired force versus displacement characteristics of the posterior and dorsal actuators. Numerical simulations illustrate the multifunctional nature of the PPy actuators and the overall power requirements of the system during the stance phase of walking gait.**

I. Introduction

THERE has been considerable research in the area of humanoid biped locomotion. However, sudden changes of direction or pace and balancing on irregular or uneven surfaces are two chief issues in biped locomotion that have not been fully addressed. The latter of these two issues is particularly challenging and can likely be solved with biologically motivated hardware and control algorithms. The central theme in this paper is the design and analysis of a foot using biomechanical insight.

Most of the existing humanoid robots are powered with DC and AC servomotors with gear heads. Unlike biological muscles, these electromechanical actuators cannot store energy and are inefficient in absorbing energy. It is known that energy storage and dissipation in human skeletal muscles plays an important role in generating efficient gait. Therefore, artificial muscle actuators having inherent compliance and damping have the potential to be effective actuators for generating natural gait.

For the present design, PPy actuators were selected among several possible artificial muscles because, like human skeletal muscle, PPy actuators can provide inherent stiffness and viscoelastic damping. They can also provide compact, low power, and low inertia actuation. Furthermore, the safety of robotics designs is enhanced by so-called "soft" polymer actuators because of their ability to yield when overloaded. Although conducting polymers have a limited control authority due to degradation by oxidation [1], small strain, and small strain rate, this paper will illustrate that a humanoid foot requires only small stroke actuation at high levels of sustained force, which are two of the positive features of PPy actuators [2], [3]. Before undertaking the design and analysis of a humanoid foot using PPy artificial muscle actuators, relevant research from robotics, PPy modeling, and biomechanics was considered.

Research surrounding humanoid robotic feet has focused primarily on traditional actuation methods applied to a single link foot. A large subset of this research deals with the associated foot to ground interaction. It is widely recognized that the gait of a biped could be enhanced by degrees of freedom distal to the ankle [4]. Specifically, multi-DOF feet allow for longer step size and a smooth, stable transition between the two feet during locomotion [5]. Another study with the same conclusion can be found in [6].

Lumped parameter models of PPy actuators are a necessary element in the design of a humanoid foot. A linear constitutive equation describing actuator electromechanical coupling was proposed by Madden in [7] and Della Santa et. al. in [8]. Madden's modeling work was extended and clarified by Bowers [9], who formulated a linear reticulated model describing the ion diffusion process, electromechanical coupling, and viscoelasticity in PPy films. Simplifications and adaptations of the foregoing models will be used in the present work to describe multilayer actuators produced by Eamex Corp. [10].

Human biomechanics serve as another key reference for the design presented in this paper. As outlined in [11], the role of muscles can be compactly defined in terms of their force versus length or work loop plot. Two representative work loops, one for positive work production and the other for energy absorption, are shown in Fig. 1. When a loop is traversed counterclockwise, energy is produced (Fig. 1a). When the loop is traversed clockwise, then energy is absorbed (Fig. 1b).

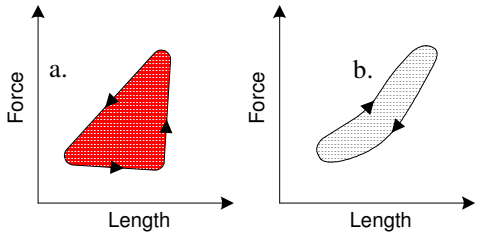

Fig. 1. a. Positive power producing work loop. b. Power absorbing work loop. Adapted from [11]

Manuscript received February 1, 2007.

T. W. Secord is a Research Assistant in the d'Arbeloff Laboratory for Information Systems and Technology at the Massachusetts Institute of Technology, Cambridge, MA 02139 USA (Phone: 617-258-0811; Fax: 617-258-3675; e-mail: secord@mit.edu).

H. Harry Asada, is a Ford Professor of Mechanical Engineering at the Massachusetts Institute of Technology, Cambridge, MA 02139 USA (e-mail: asada@mit.edu).

From a design perspective, the joint angles and ground reaction forces (GRFs) taken from biomechanics provide the information necessary to design a humanoid foot actuation scheme. Representative studies of human foot motion can be found in [12]-[15].

This paper is organized as follows. First, a low-order lumped parameter model of PPy actuators is obtained in II, followed by a kinematic and static analysis of a multi-joint foot. Time profiles of GRFs and joint trajectories are obtained from biomechanics literature, and converted into the foot's actuator coordinates. The inherent actuator compliance and damping are tuned in such a way that the net actuator effort be minimized in generating the force and displacement profiles of the desired gait. Numerical data will demonstrate the effectiveness of the method.

II. Modeling of Polypyrrole Actuators

The completed lumped parameter model used for the foot design is shown in Fig. 2. The proposed model consists of electrical and mechanical components connected by a one way coupling from the electrical to the mechanical domain. The mechanical model is further divided into a series rigid displacement generator and a Maxwell viscoelastic element. The primary aspects of the actuator model will now be discussed.

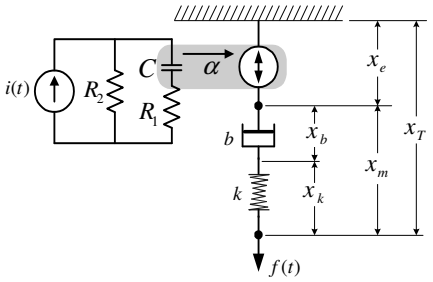

Fig. 2: Lumped parameter model of a PPy multilayer actuator

A. Charge Accumulation

Charge accumulation is modeled using the electrical circuit shown on the left-hand side of Fig. 2. This model is similar to that found in [7] and [9]. The capacitance, C, represents the bulk capacitance of the PPy film. The resistance R_1 represents the resistance associated with ion diffusion, the contact resistance of the electrodes, and the electrolyte resistance. Current leakage is modeled by an additional resistive path characterized by R_2. The first order differential equation governing the charge accumulation on the capacitor is

$$Q + (R_1 + R_2)C\dot{Q} = R_2 C i(t)\,. \tag{1}$$

B. Passive Mechanical Properties

The Maxwell model shown in the right-hand side of Fig. 2 will be used to account for the instantaneous elongation and time-integral creep after a sudden load is applied. The mechanical model is parameterized by the stiffness k and damping b. Thus, the mechanical displacement x_m is the sum of the elastic elongation x_k and viscous elongation x_b as

$$x_m = x_k + x_b = \tfrac{f(t)}{k} + \tfrac{1}{b}\int f(t)dt\,. \tag{2}$$

C. Charge Induced Strain

The electrochemical strain generated by the application of a current or voltage to a PPy film has been shown to be linearly related to the amount of charge accumulated in the material through the charge to strain ratio α [7], [8]. The linear relationship is shown in (3), where x_e is the electrochemical displacement due to charge, α is the displacement-to-charge coefficient, and Q is the charge contained on the capacitor C:

$$x_e = \alpha Q\,. \tag{3}$$

For a stress of up to 30 MPa in single films, this relationship has been shown to be relatively constant and additive to the mechanical displacement x_m. Therefore, the electrochemical displacement generating element is in series with the remainder of the mechanical model as shown in Fig. 2.

III. Foot Design and Analysis

A. Foot Design Overview

The design of the foot assembly is shown in Fig. 3. The design consists of four sections that are named anatomically as the tibia, the hindfoot, the forefoot, and the phalanges. For simplicity of analysis, only the posterior and dorsal actuators are considered in this paper. However, the design intent is to place additional anterior and plantar actuators on the foot to achieve full joint articulation. The posterior and dorsal actuators are placed to achieve effects analogous to the tendons and muscles of the anterior and posterior compartments of the human lower leg. The prototype shown in Fig. 3 was realized using a fuse-deposition-modeling printer and two 12-layer PPy actuators made by Eamex Corp. The tendon material is 0.64 mm Kevlar cord and the interdigitating foot sections were secured using 2.1 mm aluminum rods.

The joints are labeled in Fig. 3 according to their human anatomical equivalent. The ankle (A) and metatarsal-phalangeal joints are purely revolute, while the tarsal-metatarsal (TM) joint is revolute within a small neighborhood of the reference configuration shown. The TM joint is unique in that it is intended to be a passive degree of freedom that is comparatively rigid, but can aid in the storage of elastic energy upon being filled with a moderate durometer elastomer.

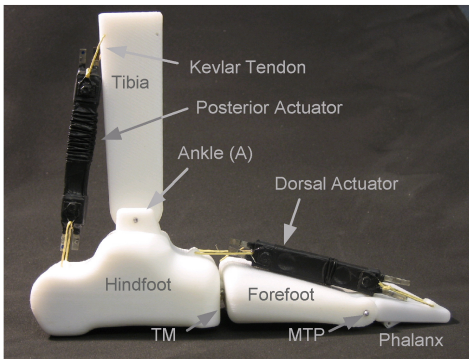

Fig. 3. Design of four degree of freedom anthropomorphic foot with artificial muscle actuators attached.

A comparison of the design in Fig. 3 with a human foot reveals many important similarities. First, the gross motion of a human foot is determined by plantar and dorsal flexion as well as rotation of the MTP joints, especially the first joint. The importance of the first MTP joint justifies its independence from the remaining MTP joints [6], which have been amalgamated into the link that is behind the phalanx in Fig. 3. Actuation of the second MTP joint is not considered in this paper. Second, the human calcaneus, or heel bone, serves as the moment arm for forces applied to the foot by the posterior leg muscles. This protuberance enables effective plantar flexion and forward locomotion both in humans and in the humanoid design.

B. Simplified Kinematic Representation of the Foot

Fig. 4 shows the nomenclature used in the computation of Jacobian matrices relating the joint space, Cartesian task space, and actuator space for the foot.

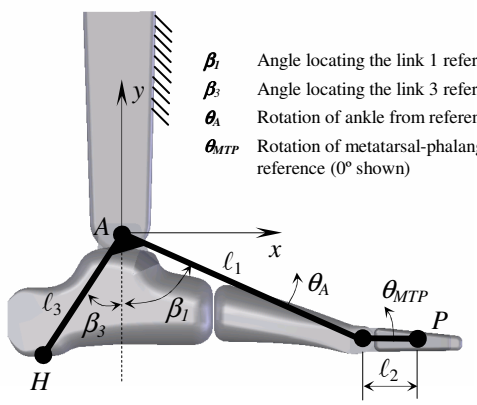

Fig. 4. Two link description of foot for consideration of ground reaction forces and actuator length changes.

Revolution about the TM joint is not included in the kinematic model because the TM joint in the present design is revolute within a small range of the neutral joint configuration. Furthermore, the TM joint is primarily a passive degree of freedom in a human foot that does not allow significant motion between the hind foot and the forefoot sections [14].

In Fig. 4, the reference coordinate system *A-xy* is attached to the leg. Note that the relevant link lengths and reference angles are provided for the points of application of the GRFs. From the perspective of the phalanx GRF which is applied at point *P*, the foot appears as a two-link manipulator. From the perspective of the heel GRF which is applied at point *H*, the foot appears only as a single link. For simplicity, the inertia of each link is assumed to be negligible.

The foregoing kinematic model allows for a straightforward assessment of the actuator force versus length characteristics. The force versus length characteristics arise from typical joint angle and GRF time histories taken from biomechanical studies of human walking. Specifically, the stance phase of gait will be considered. The stance phase can be broken down into 5 sub-phases: initial contact (of the heel), loading, midstance, terminal stance, and pre-swing (also called toe-off).

C. Actuator Lengths in a Biomimetic Stance Phase

The combined length of an actuator and tendon is a geometric constraint imposed by joint rotation in the kinematic model. This constraint indicates what x_T must be for each actuator throughout the stance phase of a walking gait. The length changes of the actuator-tendon combination can be computed using the nomenclature defined in Fig. 5 and joint angle histories provided in IV-*A*.

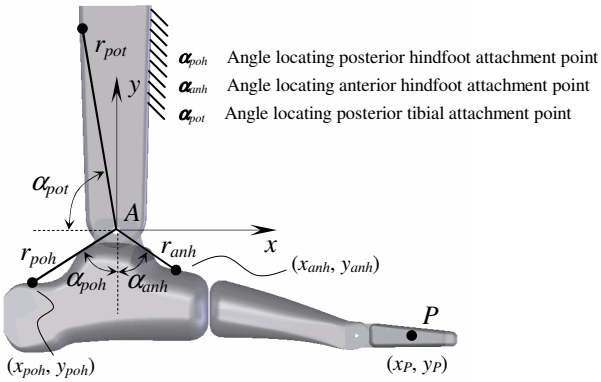

Fig. 5. Terminology relevant to the computation of actuator-tendon length changes.

Specifically, for the an actuator-tendon combination whose original length is ℓ_0, the change in length $\Delta\ell$ during is given by the L_2 norm

$$\Delta\ell = \left\| \mathbf{x}_i(\boldsymbol{\theta}(t)) - \mathbf{x}_j(\boldsymbol{\theta}(t)) \right\| - \ell_0, \qquad (4)$$

where $\mathbf{x}_i$ and $\mathbf{x}_j$ are the vectors originating at the ankle *A* and terminating and the i^{th} and j^{th} actuator attachments points respectively. Eq. (4) is applied to both the anterior actuator (indicated later in subscript by *an*) or the dorsal actuator (indicated later in subscripts as *do*). The *i* and *j* subscripts use the following two pairings: *POT* (posterior tibial) to *POH* (posterior hindfoot) and *ANH* (anterior hindfoot) to *P*

(phalanx). The order of the *i* and *j* pairings is immaterial in (4). Note that since the tendons are assumed to be rigid, $\Delta\ell = x_T$ for both actuators (see Fig. 2).

In the present model, tendon wrapping was not considered because the location of the dorsal actuator tendon attachment on the phalanx assures that tendon wrapping will only occur at angles beyond approximately 15° of relative plantar flexion between the forefoot and phlanax.

D. Actuator Forces in a Biomimetic Stance Phase

This section describes the formulations of the Jacobian matrices necessary for force analysis of the foot. Only the posterior and dorsal actuators have been considered in order to uniquely resolve the GRFs into the actuator space. Hence, the posterior and dorsal actuators must provide both compressive and tensile forces. Although this assumption becomes invalid beyond small compressive loads, the removal of two actuators simplifies the analysis and yet provides meaningful results.

The manipulator Jacobian matrix denoted by $\mathbf{J}_{\theta\to x}$ provides a convenient method for converting applied GRFs into the joint space torques. One additional Jacobian transformation is required to project the forces onto the actuator coordinate system; the necessary matrix is denoted by $\mathbf{J}_{\ell\to\theta}$ The task, joint and actuator spaces are denoted in the subscripts by *x*, θ, and ℓ respectively. Notice that the spaces *x*, θ, $\ell \subseteq \mathbb{R}^2$.

Under the assumptions listed in III-*B*, the GRFs can be transformed into actuator forces using (5):

$$\boldsymbol{f} = (\mathbf{J}^P_{\theta\to x}\mathbf{J}^P_{\ell\to\theta})^T\mathbf{F}_P + (\mathbf{J}^H_{\theta\to x}\mathbf{J}^H_{\ell\to\theta})^T\mathbf{F}_H\,, \tag{5}$$

where $\boldsymbol{f}$ is the vector of actuator forces and the vectors $\boldsymbol{F}_P$ and $\boldsymbol{F}_H$ represent the ground reaction forces applied at the points *P* and *H* respectively (see Fig. 4). Also, in (5), the Jacobians are given superscripts *P* and *H* based the force under consideration.

The Jacobian matrix relating the joint and task spaces for consideration of the phalanx GRF is defined by the partial derivatives of the force application spatial coordinate $\mathbf{x}_P$ with respect to the joint angles θ_A and θ_{MTP}. Thus

$$\mathbf{J}^P_{\theta\to x} = \begin{pmatrix} \ell_1\,\mathrm{c}(\beta_1+\theta_A) - \ell_2\,\mathrm{s}(\theta_{MTP}+\theta_A) & -\ell_2\,\mathrm{s}(\theta_{MTP}+\theta_A) \\ \ell_1\,\mathrm{s}(\beta_1+\theta_A) + \ell_2\,\mathrm{c}(\theta_{MTP}+\theta_A) & \ell_2\,\mathrm{c}(\theta_{MTP}+\theta_A) \end{pmatrix}, \tag{6}$$

where the c and s indicate sine and cosine. Similarly, for the heel GRF projection onto joint space, the necessary Jacobian matrix is

$$\mathbf{J}^P_{\theta\to x} = \begin{pmatrix} \ell_3\,\mathrm{c}(\beta_3-\theta_A) & 0 \\ -\ell_3\,\mathrm{s}(\beta_3-\theta_A) & 0 \end{pmatrix}. \tag{7}$$

The Jacobian matrices relating the actuator and joint spaces are defined by the partial derivatives of the joint angles θ_A and θ_{MTP} with respect to the actuator lengths x_T. Therefore, implicitly differentiating (4) and solving for the appropriate derivatives gives (8) and (9).

$$\mathbf{J}^P_{\ell\to\theta} = \begin{pmatrix} \frac{\partial\theta_A}{\partial X_{T,po}} & 0 \\ 0 & \frac{\partial\theta_{MTP}}{\partial X_{T,do}} \end{pmatrix} \tag{8}$$

$$\mathbf{J}^H_{\ell\to\theta} = \begin{pmatrix} \frac{\partial\theta_A}{\partial X_{T,po}} & 0 \\ 0 & 0 \end{pmatrix} \tag{9}$$

The subscripts in (6) to (9) remain as previously defined. Note that all of the required Jacobian matrices are configuration dependent. Specifically, (6) and (7) depend on the joint angles while (8) and (9) depend upon the actuator lengths as well as the joint angles.

E. Actuator Energetics

The multifunctional nature of the artificial muscles is illustrated by considering the flow of energy in the biomimetic system. Table 1 summarizes the variables used in the system power calculations. The power versus time for each lumped element can be established by multiplying the corresponding effort and flow variables as listed in Table 1.

TABLE I
VARIABLES USED TO COMPUTE INSTANTANEOUS POWER

Power	Effort	Flow	Corresponding Definition
P_k	kx_k	$\dot{x}_k$	Stored and delivered by spring
P_b	$b\dot{x}_b$	$\dot{x}_k$	Dissipated in damper
P_F	f	$\dot{x}_T$	Input arising from GRFs
P_C	$\frac{Q}{C}$	$\dot{Q}$	Stored and delivered by capacitor
P_R	V_{R1}, V_{R2}	i_{R1}, i_{R2}	Dissipated in resistances
P_I	V_{R2}	$i(t)$	Input by electrical power supply

IV. Numerical Simulation

A. Actuator Force and Displacement Characteristics

Lower body joint angles and GRFs have been extensively quantified in biomechanics literature for the stance phase of walking. The GRFs and joint angles used in subsequent numerical simulations are shown in Fig. 6. The GRF profiles are based on data shown in [13] and scaled to 10% of the human amplitude of 1kN. The 10% scaling assures that the forces in the actuators are within achievable limits. The joint angles shown were obtained using polynomial approximations to data provided in [14].

Typical ground reaction forces exhibit a two peak response that can be approximated as the sum of two sine waves as shown in middle and lower plots in Fig. 6. These force approximations are similar to those found in [15]. The distribution of GRFs across the foot was quantified by assuming that the center of pressure (COP) traveled forward from the heel to the toe linearly with time.

The length and force characteristics versus time were computed for each actuator based on the biomechanical data. The length versus time was computed using (4) and the joint angles shown in Fig. 6. The force versus time was computed using (5) and the GRFs shown in Fig. 6. Fig. 7 shows the resulting work loop diagram. Note that the

spacing between the data points in Fig. 7 reflects equal time intervals.

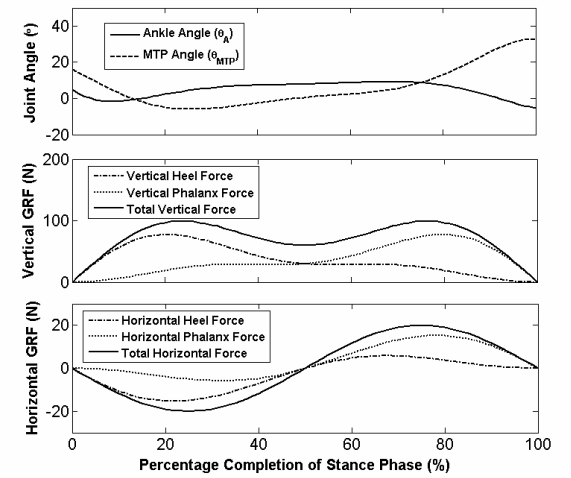

Fig. 6. Joint angles and GRFs taken from biomechanical studies of human walking. [13], [14]

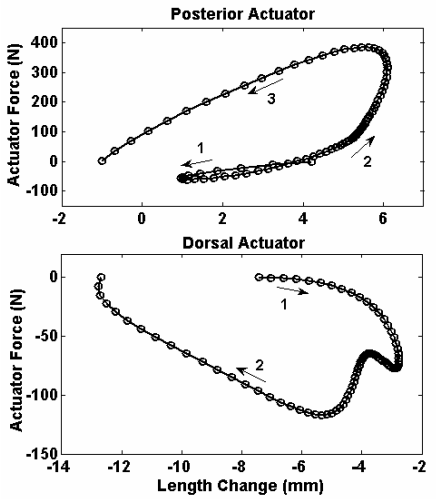

Fig. 7. Force versus length characteristics for the posterior and dorsal actuators as computed from biomechanical GRFs and joint angles.

The upper plot in Fig. 7 shows that for the posterior actuator the total length quickly decreases in response to the applied force at the heel. The actuator then must elongate isotonically until the arrow labeled 2 at which time it must sustain a large tensile force isometrically until it begins to rapidly shorten indicating the terminal stance and pre-swing of the foot. The counter-clockwise motion of the curve indicates that the posterior actuator enables the foot to perform work on the environment.

The dorsal actuator begins in a compressive state during the heel strike and initially elongates as the foot rolls forward. As required by (4), the dorsal actuator must shorten throughout the remainder of the stance phase. However, the actuator force simultaneously decreases. This indicates that the dorsal actuator must be very stiff and act primarily as a displacement generator and energy dissipation element. The dissipative nature of the actuator is also present in the clockwise motion of the force versus length curve. Explicit quantification of the required stiffness and damping is provided in the next section.

B. Selection of Optimal Actuator Stiffness and Damping

The force versus length characteristics described in IV-*A* represent the actuator behavior required to reproduce the biomechanical joint motions for the given set of GRFs. Thus, the k and b parameters for each actuator must be selected to provide a passive response that matches Fig. 7 as closely as possible. The displacement discrepancy that remains must be forced to zero using the rigid displacement generator that behaves according to (3). The error between the passive response and will be treated as the required feed-forward input to achieve a biomimetic stance phase.

The optimal stiffness and damping within maximum and minimum limits are given by

$$(k,b)_{opt} = \underset{\substack{k_{\min}\le k\le k_{\max}\\ b_{\min}\le b\le b_{\max}}}{\arg\min} \sum_{t=1}^{N} (x_m(k,b,\boldsymbol{f}(\mathbf{F}_P,\mathbf{F}_H)) - \Delta\ell(\theta))^2 \quad (10)$$

where $\Delta\ell(\theta)$ is the desired length profile computed from (4), $\boldsymbol{f}(\boldsymbol{F_P}, \boldsymbol{F_H})$ is the actuator force vector given by (5), and N is the total number of data points used in the stance phase calculations. In words, (10) says that the optimal stiffness k and optimal damping b will minimize the squared error between the mechanical length as computed from (2) using the actuator forces $\boldsymbol{f}(\boldsymbol{F_P}, \boldsymbol{F_H})$ and the desired biomimetic length $\Delta\ell(\theta)$ as computed from (4) using the biomechanical joint angle data. Eq. (10) was evaluated using Matlab to find the local minimum in the search space $k \in (1, 1\times10^9)$ *N/m* and $b \in (1, 1\times10^9)$ *N·s/m*. The results are shown in Table 2.

TABLE II
OPTIMAL STIFFNESS AND DAMPING FOR BIOMIMETIC DESIGN

Actuator	k (*N/m*)	b (*N·s/m*)	Remarks
Posterior	9.46×10^4	2.78×10^4	
Dorsal	∞	1.32×10^5	∞ indicates > 1×10^9

Notice that the posterior actuator possesses optimal compliance and damping values that are much smaller than those required in the dorsal actuator. These values are slightly beyond the achievable range of various commercially available actuators [10]. Recall that the values in Table 2 arise from GRFs that are scaled to 10% of typical human values. The passive mechanical response of the posterior actuator using the optimal stiffness and damping resulted in an average feed-forward correction of –0.5 mm. In contrast, the dorsal actuator required an average feed-forward correction of 2 mm.

C. Power versus Time During Stance Phase

The power versus time was computed for each lumped parameter element in the system using Table 1. Note that the feedforward displacement obtained in Section IV-*B* was converted into the equivalent feedforward current $i(t)$ using (2) and (3). The electrical power and energy stored were

computed using R_1 = 0.4 Ω, R_2 = 2.4 Ω, and C = 2.7 F. These parameter values were computed for a 12 layer actuator using the techniques described in [16] and [17]. The power versus time results are shown in Fig. 8 for the posterior actuator.

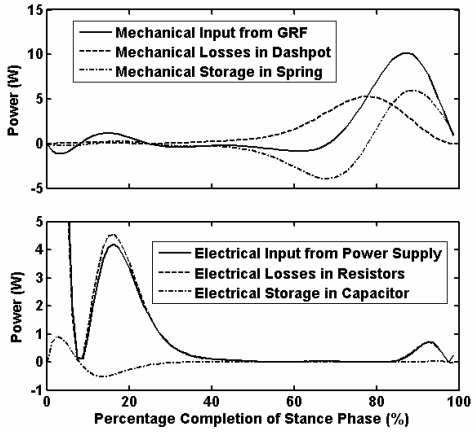

Fig. 8. Power input, storage, and dissipation during stance phase for posterior actuator.

The upper plot in Fig. 8 shows that the spring is effective as an energy storage element because the amplitude of the power flowing into and out of the spring is a significant fraction of the power introduced into the system by the GRFs, especially beyond 50% completion of the stance phase. Similarly, the damping is also crucial for biomimetic behavior as evidenced by the large 5 W dissipative peak occurring between 60% and 80% of the stance phase.

The lower plot in Fig. 8 illustrates that the posterior actuator requires a large power spike during the initial contact and loading of the stance phase but requires very little power thereafter. Moreover, current PPy technology entails large resistive losses. Although not explicitly computed, system power requirements can be obtained by integrating the electrical power input $P_I = V_{R2} \cdot i(t)$ with respect to time for the duration of a single stride. This result is then multiplied by twice the stride frequency to yield the bipedal foot power consumption.

V. Conclusion

A humanoid foot has been designed and analyzed using biomechanical joint angles and GRFs. The biomechanical data were converted to the actuator space force and length variables. Using the resulting actuator forces, stiffness and damping parameters were selected to minimize the error between the passive mechanical response length and the length profiles required by the biomechanical data. The optimal posterior actuator must be compliant and dissipative throughout the stance phase while the dorsal actuator must be very stiff and dissipative. The electrical and mechanical power implications of the design were also addressed for the posterior actuator. The mechanical power was found to be on the order of 10 W throughout most of the stance phase.

The results in IV show that a biomimetic design can be successfully obtained and interpreted in the language of biomechanics. Future work will focus on considering antagonistic actuators placed on the foot as well as other actuation modalities.

Acknowledgment

This material is based upon work supported by the National Science Foundation under Grant No. 0413242.

References

[1] Otero T.F., Marquez M., Suarez I., "Polypyrrole: Diffusion Coefficients and Degradation by Overoxidation", *J. Phys. Chem.*, B, Vol. 108, pp. 15429-15433, 2004.

[2] Zama T., Hara S., Takashima W., Kaneto K., "Comparison of Conducting Polymer Actuators Based on Polypyrrole Doped with BF_4^-, PF_6^-, $CF_3SO_3^-$, and ClO_4^-," *Bull. Chem. Soc. Jpn.*, Vol. 78, pp. 506-511, 2005.

[3] Kaneto K., Nakashima M., Takashima W., "Improvement of electrochemical deformation of conducting polymers, strain, force, and response," *Proceedings of the SPIE 11th Annual Symposium on Smart Structures and Materials: Electroactive Polymer Actuators and Devices*, Yoseph Bar-Cohen, Ed., pp. 190-198, SPIE, Bellingham WA, 2004.

[4] Ouezdou F.B., Alfayad S., and Almasri B., "Comparison of Several Kinds of Feet for Humanoid Robot", *Proceedings of the IEEE-RAS International Conference on Humanoid Robots*, pp. 123-128, 2005.

[5] Bruneau O., Ouezdou F.B., and Fontaine J.G., "Dynamic Walk of a Bipedal Robot Having Flexible Feet", *Proceedings of the IEEE / RSJ- International Conference on Intelligent Robots and Systems*, pp. 512-517, 2006

[6] Takamura H. et. al., "Study of the Toes Role in Human Walk by Toe Elimination and Pressure Measurement System", *Proceedings of the IEEE International Conference on Systems, Man and Cybernetics*, Vol. 3, pp. 2569-2574, 2003.

[7] Madden J.D., "Conducting Polymer Actuators", *Ph.D. Thesis*, Massachusetts Institute of Technology, Cambridge, MA, 2000.

[8] Della Santa A., De Rossi D., Mazzolidi A., "Characterization and modeling of a conducting polymer muscle-like linear actuator", *Smart Materials and Structures*, Vol 6, pp. 23-24, 1997.

[9] Bowers T.A., Anquetil P., Hunter I., Hogan N., "Analysis and Modeling of Electro-Mechanical Coupling in an Electroactive Polymer-Based Actuator," *Materials Research Society Symposium Proceedings*, Vol 785, D.5.6.1-D.5.6.6, 2004.

[10] http://www.eamex.co.jp/denshi_hp/english/denshi_idex_e.htm

[11] Dickinson M.H., Farley C.T., Full R.J., Koehl M.A.R, Kram R., Lehman S. "How Animals Move," *Science*, Vol. 288, pp. 100-106, 2000.

[12] E. Salathe, G.A. Arangio "A Biomechanical Model of the Foot: The Role of Muscles, Tendons, and Ligaments," *Journal of Biomechanical Engineering*. Vol. 122, pp. 281-287, 2000.

[13] Winter D.A., Gilchrist L.A., "A Two-Part, Viscoelastic Foot Model For Use In Gait Simulations", *Journal of Biomechanics*, Vol. 29, No. 6, pp. 795-798, 1996.

[14] Carson M.C. et. al., "Kinematic analysis of a multi-segment foot model for research and clinical applications: a repeatability analysis", *Journal of Biomechanics*, Vol. 34, pp. 795-798, 1996.

[15] Kram R. and Powell A.J., "A treadmill-mounted force platform", Journal of Applied Physiology, Vol. 67, Issue 4, 1692-1698, 1989.

[16] Secord T.W., "Modeling, Identification, and Application of Multilayer Polypyrrole Conducting Polymer Actuators", *S.M. Thesis*, Massachusetts Institute of Technology, Cambridge, MA, 2007.

[17] McCombie D.B., Secord T.W., Asada H.H., "Modeling and Observer Design for Polypyrrole Conducting Polymer Actuator Control Systems", *Proceedings of the IEEE / RAS-EMBS International Conference on Biomedical Robotics and Biomechatronics*, pp. 432-436, 2006